LETTERS IN BIOMATHEMATICS
An International Journal

Intercollegiate Biomathematics Alliance

RESEARCH ARTICLE

OPEN ACCESS

Numerical Approaches to Division and Label Structured Population Models

Fabian Santiago[a], Kevin B. Flores[b], Suzanne S. Sindi[a]

[a]Department of Applied Mathematics, School of Natural Sciences, University of California, Merced, CA, USA;
[b]Department of Mathematics, North Carolina State University, Raleigh, NC, USA

ABSTRACT

Division and label structured population models (DLSPMs) are a class of partial differential equations (PDEs) that have been used to study intracellular dynamics in dividing cells. DLSPMs have improved the understanding of cell proliferation assays involving measurements such as fluorescent label decay, protein production, and prion aggregate amplification. One limitation in using DLSPMs is the significant computational time required for numerical approximations, especially for models with complex biologically relevant dynamics. Here we develop a novel numerical and theoretical framework involving a recursive formulation for a class of DLSPMs. We develop this framework for a population of dividing cells with an arbitrary functional form describing the intracellular dynamics. We found that, compared to previous methods, our framework is faster and more accurate. We illustrate our approach on three common models for intracellular dynamics and discuss the potential impact of our findings in the context of data-driven methods for parameter estimation.

ARTICLE HISTORY
Received July 28, 2020
Accepted October 1, 2020

KEYWORDS
Structured population model, PDEs, high dimensional integrals, recursive numerical integration

1 Introduction

Division and label structured population models have recently been investigated in the context of cell proliferation assays. These assays yield insight into the role of cell cycle dynamics (Smith and Martin, 1973) and intercellular heterogeneity (Glauche et al., 2009) to the overall growth of a population of cells. A widely used proliferation assay, developed by Lyons and Parish (1994), uses the intracellular dye carboxyfluorescein succinimidyl ester (CFSE). CFSE is nonradioactive and enables a durable and sufficiently uniform labeling of a population of cells without adverse effects on proliferation and death. Label structured population models are an ideal tool for understanding these type of data because the CFSE dye is modeled as a label that is approximately partitioned into two equal halves when cells divide into two daughter cells. Flow cytometry can be used to rapidly measure CFSE fluorescence intensity for each cell in a population (Lyons and Parish, 1994; Lyons et al., 2001; Parish, 1999; Quah et al., 2007; Wallace et al., 2008; Witkowski, 2008), resulting in a population histogram. Peaks in the histogram are typically interpreted to represent a separate generation of cells, i.e., the number of times a subpopulation of cells has divided. Prior to the application of division and structured population models to CFSE data (Banks et al., 2011,a; Luzyanina et al., 2009a, 2007), the number of cells in each generation was approximated using simple binning or deconvolution techniques (De Boer et al., 2006; De Boer and Perelson, 2005; Deenick et al., 2003; Ganusov et al., 2005; Gett and Hodgkin, 2000). CFSE labeling has been used to study immune system dynamics through monitoring lymphocytes proliferation (Lyons and Parish, 1994) and is also able to track the proliferation behavior of specific types of lymphocytes through the use of fluorescent antibodies with specificity to markers on the lymphocyte cell surface (Lyons et al., 2001). The typical response of various cell populations within the immune system is to clonally expand when presented with foreign antigens. Thus, being able to more accurately quantify these responses, e.g., by estimating rates of activation, proliferation, and death through coupling structured population models with data, will lead to a more complete characterization of how various diseases and stimuli affect the immune system. With increasing advances in the ability to quantify the contents in single-cells (Marx, 2019), such structured population models will become more applicable.

Previous efforts to fit CFSE label decay experimental data with division and label structured population models used a least squares inverse problem framework (Luzyanina et al., 2009b, 2007; Banks et al., 2011,b). The inverse problem formulation typically involves estimating parameters by minimizing a least squares cost function that measures the discrepancy between a

CONTACT Suzanne S. Sindi ssindi@ucmerced.edu

solution of the PDE system at a set of parameter values and the histogram data from flow cytometry. Optimization routines that have been used to solve the inverse problem with flow cytometry data include derivative free methods (Luzyanina et al., 2007), such as the Nelder-Mead simplex based method, and gradient based methods relying on the computation of a local gradient of the cost function (Banks et al., 2012). Both of these optimization methods use an iterative scheme requiring thousands of simulations of the forward solution of the label structured PDE system at different parameter values. In the case where division structure is modeled with separate compartments, i.e., one per cell division cycle, the computational requirements are exacerbated since one needs to solve a large system (>10) of coupled PDEs. Under simplifying assumptions on the form of the CFSE label decay rate, such as decay that is directly proportional to the amount of intracellular label, analytical solutions to the PDEs can be obtained through the method of characteristics. The main drawbacks to these assumptions are that the resulting decay rate functional forms may not accurately explain the data and that they do not extend to other scenarios involving the measurement of an intracellular label such as protein production (Blake et al., 2003; Flores, 2013a) or prion aggregate amplification (Banks et al., 2018). Thus, more efficient numerical methods are needed to enable validation of division and labeled structured population models from data across a broader range of assumptions describing the rate of change of the intracellular label.

In this work, we develop a novel numerical and theoretical framework for a class of division and label structured population models. We develop our framework in the more general context of population of dividing cells that is structured by the concentration of a single intracellular species evolving under its own dynamics (rather than a decaying label). In Section 2, we derive a recursive relation allowing the density of the $(i+1)$-generation to be solved in terms of the i^{th} generation. In Section 3 we apply our recursive formulation to three common models for intracellular dynamics. In Section 3.3.2 we demonstrate that our recursive framework facilitates rapid and accurate numerical solutions through recursive numerical integration. In Section 4 we summarize our findings and discuss their implications in the context of parameter inference and uncertainty quantification.

2 Solutions to Division and Label Structured Population Model

We seek to model the concentration of a single intercellular constituent in a population of actively dividing cells. Let $a(t)$ be the concentration of an intracellular species in a cell t hours after the start of an experiment. In the absence of division, the intracellular dynamics are governed by the following ordinary differential equation

$$\frac{da}{dt} = I(a;\theta), \tag{1}$$

where I is assumed to be a known smooth function of possibly unknown parameters (θ). When cells divide, the intracellular constituent is divided between daughter cells. Let $Y_i(t,a)$ represents the constituent density of cells that have undergone i cell divisions since the beginning of the experiment. The dynamics of each generation in the dividing cellular population evolves according to the following system of coupled partial differential equations:

$$\begin{aligned}
\frac{\partial}{\partial t}Y_0(t,a) + \frac{\partial}{\partial a}(I(a;\theta)Y_0(t,a)) &= -(\alpha_0(t)+\beta_0(t))Y_0(t,a),\\
\frac{\partial}{\partial t}Y_1(t,a) + \frac{\partial}{\partial a}(I(a;\theta)Y_1(t,a)) &= -(\alpha_1(t)+\beta_1(t))Y_1(t,a) + 2\gamma\alpha_0(t)Y_0(t,\gamma a),\\
&\vdots\\
\frac{\partial}{\partial t}Y_M(t,a) + \frac{\partial}{\partial a}(I(a;\theta)Y_M(t,a)) &= -(\alpha_M(t)+\beta_M(t))Y_M(t,a) + 2\gamma\alpha_{i-1}(t)Y_{i-1}(t,\gamma a),
\end{aligned} \tag{2}$$

where $\alpha_i(t)$ and $\beta_i(t)$ represent the division and death rates respectively. As mentioned above i represents the number of divisions since the beginning of the experiment (not the generational age) and so our problem formulation includes the following initial conditions:

$$Y_0(0,a) = \Upsilon(a) \quad \text{and} \quad Y_i(0,a) = 0 \quad \text{for } i \geq 1. \tag{3}$$

Where $\Upsilon(a)$ is the initial constituent density of cells at the start of an experiment. Following previous convention we refer to this system as the Division and Label Structured Population Model (DLSPM).

In this study, we derive solutions to the DLSPM (Equations (2) & (3)) through recursive integration of the previous generation. The decomposition approach for finding solutions to $Y_i(t,a)$ in terms of $\Upsilon(a)$, used in Theorem 2.1 of Banks et al. (2016) and first presented in Hasenauer et al. (2012), is valid only for functions of the form $I(a;\theta) = v(t;\theta)a$. Theorem 1 stated below is valid for a broader set of flux functions, namely those which allow for solution via the method of characteristics, and whose characteristics are invertible. This includes the flux functions considered by Hasenauer et al. (2012).

Theorem 1. *The solution of the system defined by Equation (2) with initial conditions in Equation (3), is given by an analytic solution and a recursive integral equation:*

$$\begin{aligned} Y_0(t,a) &= \Upsilon(s(t,a))\mu_0(t,s(t,a))^{-1} \quad \textit{and} \\ Y_i(t,a) &= \frac{2\gamma\alpha_{i-1}(t)}{\mu_i(t,s(t,a))}\int_0^t \mu_i(\tau,s(t,a))Y_{i-1}(\tau,\gamma a(\tau,s(t,a)))d\tau \quad \textit{for} \, 1 \le i \le M \end{aligned} \tag{4}$$

in which

1. *$s(t,a)$ comes from solving the characteristic equation:*

$$\frac{da}{dt} = I(a;\theta) \tag{5}$$

   with the parametric initial condition $a(0,s) = s$ and

2. *$\mu_i(t,s)$ is an integration factor of the form*

$$\mu_i(t,s) = \exp\left(\int_0^t \alpha_i(\tau) + \beta_i(\tau) + \frac{dI(a;\theta)}{da}\Big|_{a=a(\tau,s)} d\tau\right). \tag{6}$$

Before presenting the proof of Theorem 1 we offer two comments on its use. First, we note it is possible to write $Y_i(t,a)$ as an explicit high dimensional integral equation of Υ; however, because the notation is cumbersome we omit it from the presentation. Second, the integral form of the solution requires being able to explicitly solve for and invert the characteristic equation (1).

Proof. To determine the solution of the linear system defined by Equation (2) with initial conditions, Equation (3), we solve these using the method of characteristics following Pinchover and Rubinstein (2005). For the initial generation $Y_0(t,a)$, we solve the characteristic equations

$$\frac{da}{dt} = I(a;\theta) \quad \text{and} \quad \frac{dY_0}{dt} + \left(\alpha_0(t) + \beta_0(t) + \frac{dI(a;\theta)}{da}\right) Y_0 = 0 \tag{7}$$

with parametric initial conditions $a(0,s) = s$ and $Y_0(0,s) = \Upsilon(s)$, respectively. Note that solution to the second characteristic equation can be written using an integrating factor. Then combining the solutions to the ODEs (Equations (7)) and the initial conditions, the solution to the initial generation $Y_0(t,a)$, is given by

$$Y_0(t,a) = \mu_0(t,s(t,a))^{-1}\Upsilon(s(t,a)) \quad \text{where} \quad \mu_0(t,s) = \exp\left(\int_0^t \alpha_0(\tau) + \beta_0(\tau) + \frac{dI(a;\theta)}{da}\Big|_{a=a(\tau,s)} d\tau\right).$$

For generations $1 \le i \le M$, we solve the characteristic equations

$$\frac{da}{dt} = I(a;\theta) \quad \text{and} \quad \frac{dY_i}{dt} + \left(\alpha_i(t) + \beta_i(t) + \frac{dI(a;\theta)}{da}\right) Y_i = 2\gamma\alpha_{i-1}(t)Y_{i-1}(t,\gamma a(t,s)) \tag{8}$$

with parametric initial conditions $a(0,s) = s$ and $Y_i(0,s) = 0$. Solving the second equation using an integrating factor and using the solution on the first equation in the system of ODEs (Equations (8)), the solution to the i^{th} generation $Y_i(t,a)$, is given by

$$Y_i(t,a) = \frac{2\gamma\alpha_{i-1}(t)}{\mu_i(t,s(t,a))}\int_0^t \mu_i(\tau,s(t,a))Y_{i-1}(\tau,\gamma a(\tau,s(t,a)))d\tau, \tag{9}$$

where

$$\mu_i(t,s) = \exp\left(\int_0^t \alpha_i(\tau) + \beta_i(\tau) + \frac{dI(a;\theta)}{da}\Big|_{a=a(\tau,s)} d\tau\right). \qquad \square$$

3 Analytic and Numerical Solutions

In this section we apply Theorem 1 to three biologically relevant intracellular models: (1) linear growth, (2) constant growth and linear decay, and (3) logistic growth. In each case, we first derive the problem specific recursive integral formulation and then compare the stability of numerical solutions using recursive numerical integration (RNI) (Ammon et al., 2016) to the explicit Lax-Wendroff (LxW) method (Shampine, 2005), a standard numerical approach for hyperbolic PDEs.

Flux Term	Average Runtime (s)			
	LxW_1	LxW_2	RNI	Exact
Linear Growth	11.1620	870.7137	0.3205	0.0559
Constant Growth and Linear Decay	0.09089	7.0570	180.6480	—
Logistic	0.4466	31.9893	0.2792	—

Table 1: Average runtimes for numerical solutions and evaluation time of the analytic solution with a linear growth, using two numerical methods Lax-Wendroff (LxW) and Recursive Numerical Integration (RNI), for three different flux terms: Linear Growth (Section 3.1), Constant Growth with Linear Decay (Section 3.2), and Logistic Growth (Section 3.3). These averages were computed over four different model evaluation times $T = 1, 2, 3$, and 4 hours.

Theorem 1 gives an analytic solution for the initial generation, however iterative substitution of previous generations to determine the following generation in the recursive formulation leads to high dimensional integral solutions that need to be numerically estimated, which requires high computational overhead. The application of RNI takes advantage of the recursive formulation in Theorem 1 and allows for numerical estimations of the structured population density by recursively iterating through previous generations until the initial generation (analytic solution) is reached. In what follows, we compare our numerical solutions for both each generation $Y_i(t,a)$ and, when informative, the "total population" which we define as the sum of densities up to some generation M:

$$Z_M(t,a) = \sum_{i=0}^{M} Y_i(t,a). \tag{10}$$

Note that Theorem 1 combined with RNI leads to a meshfree method that allows for the evaluation of each generation at a single point in terms of intracellular constituent level and time (t,a), which is not possible with methods, such as LxW, that require a spatial grid. In this implementation of RNI, Guass-Legendre quadrature (von Winckel, 2004) is applied for solving the integral equations. In order to compare RNI to LxW numerical solutions, the number of Gauss-Legendre quadrature points were determined systematically as we detail in the Appendix. Briefly, the number of quadrature points were increased until the addition of a new quadrature point did not lead to an appreciable change in the solution. Also, the same number of quadrature points were used for integration at every level of recursion.

Intriguingly, for our third example the number of quadrature points needed per generation decreased while for our second example the number of points increased. Therefore, in this work, RNI outperformed LxW with intracellular dynamic models with a linear and logistic growth flux terms, but not in the case of a flux that consisted of constant synthesis and linear degradation (Table 1). Because of this, we conjecture that using Theorem 1 and RNI will outperform LxW in terms of accuracy and speed when the flux term, Equation (1), does not have a constant non-zero additive or degradation term.

3.1 Linear Growth

We first consider linear growth of an intracellular constituent:

$$I(a;\theta) = v(t;\theta)a. \tag{11}$$

In this case, an analytic solution is known from the decomposition method first presented in Hasenauer et al. (2012). We recover the same solution in our recursive integral formulation and use the analytic solution to compare to our numerical solutions with RNI and LxW.

3.1.1 Recursive Integral Formulation

We present the general solution to Equation (2) with initial conditions stated in Equation (3) and $I(a;\theta)$ as in Equation (11). To apply Theorem 1 we solve the following equation:

$$\frac{da}{dt} = v(t;\theta)a \tag{12}$$

with the parametric initial condition $a(0,s) = s$. This yields $a(t,s) = s\exp\left(\int_0^t v(t;\theta)dt\right)$ and $s(t,a) = a\exp\left(-\int_0^t v(t;\theta)dt\right)$. We then solve

$$\mu_i(t,s) = \exp\left(\int_0^t \alpha_i(\tau) + \beta_i(\tau) + \frac{dI(a;\theta)}{da}\Big|_{a=a(\tau,s)} d\tau\right).$$

This is simply $\mu_i(t,s) = \exp\left(\int_0^t \alpha_i(\tau) + \beta_i(\tau) + v(\tau;\theta)d\tau\right)$. Then the analytic solution to the initial generation, $Y_0(t,a)$, is

$$Y_0(t,a) = \mu_0(t,s(t,a))^{-1}\Upsilon\left(a\exp\left(-\int_0^t v(\tau;\theta)d\tau\right)\right). \tag{13}$$

Then from Theorem 1, we have that $Y_i(t,a)$ is given by

$$Y_i(t,a) = \frac{2\gamma\alpha_{i-1}(t)}{\mu_i(t,s(t,a))}\int_0^t \mu_i(\tau,s(t,a))Y_{i-1}(\tau,\gamma a(\tau,s(t,a)))d\tau. \tag{14}$$

For simplicity we consider constant cell division and constant cell death rates, $\alpha_i(t) = \alpha$ and $\beta_i(t) = \beta$, where $\alpha,\beta \geq 0$, for $0 \leq i \leq M$, and we have $\mu_i(t,s) = \mu(t,s) = \exp((\alpha+\beta)t)\exp\left(\int_0^t v(\tau;\theta)d\tau\right)$. We drop the subscript notation because there is no longer a dependence on the generation i. We can then write the initial solution

$$Y_0(t,a) = \mu(t,s(t,a))^{-1}\Upsilon\left(a\exp\left(-\int_0^t v(\tau;\theta)d\tau\right)\right).$$

Now we can write the first generation as

$$Y_1(t,a) = \frac{2\gamma\alpha}{\mu(t,s(t,a))}\int_0^t \mu(\tau,s(t,a))Y_0(\tau,\gamma a(\tau,s(t,a)))d\tau.$$

When we substitute $Y_0(t,a)$ we see that

$$Y_1(t,a) = \frac{2\gamma\alpha}{\mu(t,s(t,a))}\int_0^t \Upsilon(\gamma s(t,a))d\tau = \frac{2\gamma\alpha t}{\mu(t,s(t,a))}\Upsilon(\gamma s(t,a)),$$

where the integrand term $\Upsilon(\gamma s(t,a))$ does not depend on τ so we can perform the integration. Further replacement of the terms $s(t,a)$ and $\mu(t,a)$, we have an analytic solution for the first generation

$$Y_1(t,a) = 2\gamma\alpha t\exp(-(\alpha+\beta)t)\exp\left(-\int_0^t v(\tau;\theta)d\tau\right)\Upsilon\left(\gamma a\exp\left(-\int_0^t v(\tau;\theta)d\tau\right)\right). \tag{15}$$

Continuing iteratively by substitution of the previous solution in the recursive integral form of Equation (14) to determine the following generation we find that

$$Y_i(t,a) = \frac{(2\gamma\alpha t)^i}{i!}\exp(-(\alpha+\beta)t)\exp\left(-\int_0^t v(\tau;\theta)d\tau\right)\Upsilon\left(\gamma^i a\exp\left(-\int_0^t v(\tau;\theta)d\tau\right)\right), \tag{16}$$

for $1 \leq i \leq M$. As expected we have reproduced the solution to this problem presented in Hasenauer et al. (2012). Note that in this case, iterative substitutions of previous generations to compute the following generations leads to an explicit analytic solution and not high dimensional integral equations as we will see in Sections 3.2 and 3.3 with different intracellular dynamics models.

3.1.2 Numerical Solution

Numerically solving the DLSPM with a linear flux (Equation (11)) requires specifying several parameters in our model. For these numerical experiments we assumed that there is no cell death ($\beta_i(t) = 0$) and a time-independent rate of cell division ($\alpha_i(t) = \log(2)/1.5$). We solved the DLSPM up to generation $M = 7$ on spatial grids of intracellular constituents that range from zero to one-hundred ($a \in [0,100]$). The spatial discretizations for Lax-Wendroff for comparison with RNI are $\Delta a = 0.1$ (LxW$_1$) and $\Delta a = 0.01$ (LxW$_2$). Recursive numerical integration is applied on the same intracellular constituent values as LxW$_1$. For simplicity, we consider a flux term that is linear in intracellular concentration $I(a;\lambda) = \lambda a$ with $\lambda = 1.5$. The number of initial cells was set equal to 1 and the initial intracellular density, $\Upsilon(a)$, was set to a normal distribution with mean 1 and variance 0.1.

For the LxW method, the CFL condition for stability that requires that $\Delta t < \frac{\Delta a}{(M+1)\cdot\max_a\{\lambda a\}} = \frac{\Delta a}{(M+1)\lambda a_{\max}}$. Here $a_{\max}$ is the largest concentration of intracellular constituent considered in the spatial discretization. The number of quadrature points used in our implementation of RNI and our systematic way of determining them are presented in the Appendix. In this case, at most four quadrature points were applied in this implementation of RNI.

We now compare numerical solutions with RNI using Theorem 1 and the application of LxW on the original DLSPM, Equation (2), to the known analytic solution to this system. As shown in Figures 1 and 2, using Theorem 1 and RNI leads greater accuracy than a LxW method at equal mesh size with a significantly faster runtime. Figure 2 and Table 2 show that RNI and the exact model evaluation significantly outperform both applications of LxW in terms of runtime.

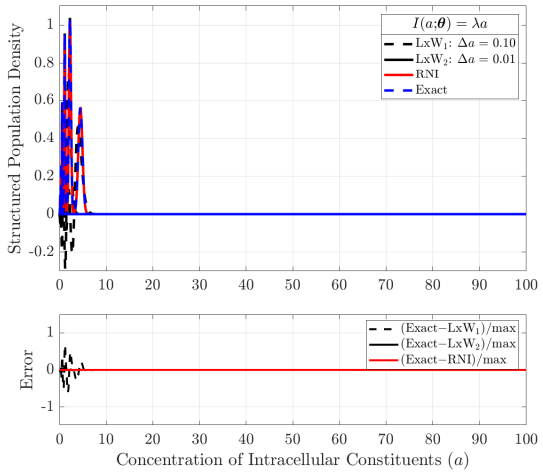

(a) $T = 1$ hour of experimental time.

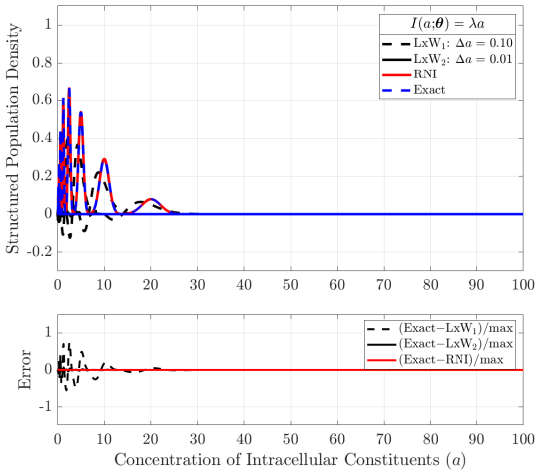

(b) $T = 2$ hour of experimental time.

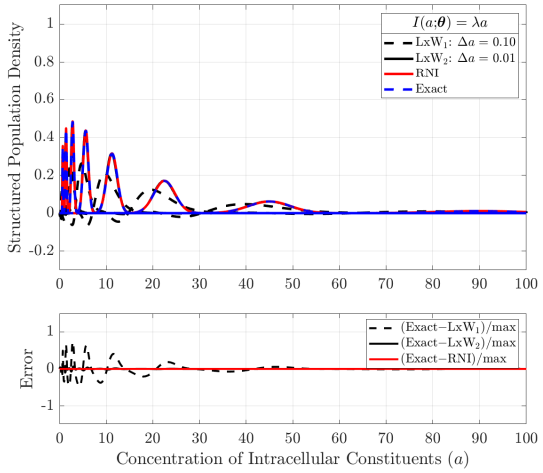

(c) $T = 3$ hours of experimental time.

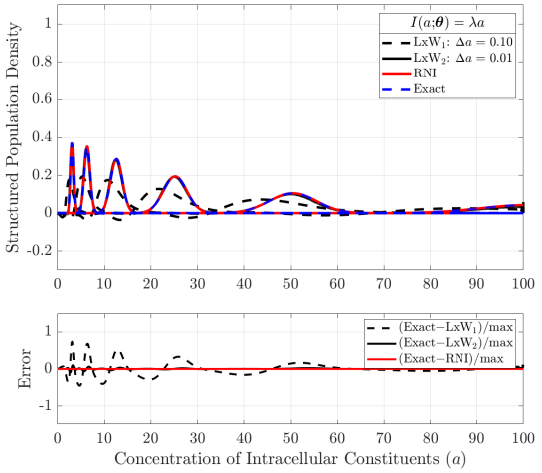

(d) $T = 4$ hours of experimental time.

Figure 1: **Numerical Solutions Linear Growth: Separate Generations.** We compare numerical solutions (RNI, LxW) of the DLSPM, (Equations (2)–(3)) with Linear Flux Term (Equation (12)) to the exact solution. (Top) We separately plot each generation at different points in time $T = 1$, 2, 3, and 4 hours. For the LxW method we used a uniform mesh with $\Delta a = 0.1$ (LxW$_1$) and $a = 0.01$ (LxW$_2$), and we used $\Delta a = 0.01$ for the RNI method. (Bottom): The error between the exact solution and each of the two numerical methods LxW and RNI. (See Section 3.1 for further details).

Method	**Runtime (s)**			
	$T = 1$	$T = 2$	$T = 3$	$T = 4$
LxW$_1$	5.528	8.812	13.17	17.14
LxW$_2$	350.6	706.6	1043.0	1383.0
RNI	0.3545	0.3636	0.2853	0.2784
Exact	0.07435	0.0435	0.04969	0.05625

Table 2: **Numerical Runtimes Linear Growth.** Runtimes for numerical solutions and evaluation time of the analytic solution for the DLSPM, (Equations (2)–(3)) with a linear flux term (Equation (11)) at four different model evaluation times $T = 1$, 2, 3, and 4 hours.

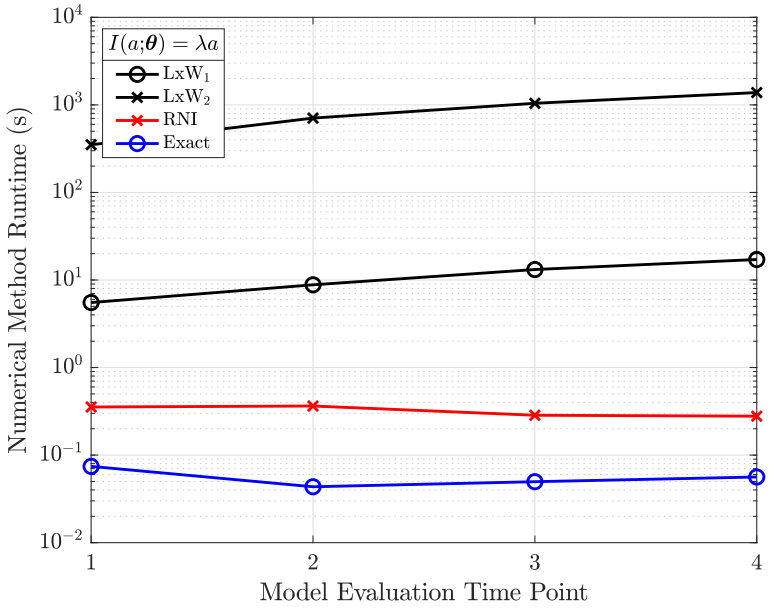

Figure 2: **Numerical Runtimes Linear Growth.** Comparison of runtimes for numerical solutions (LxW and RNI) and the exact solution (Hasenauer et al., 2012) for the DLSPM (Equations (2)–(3)) with a linear flux term (Equation (11)) at four different model evaluation times $T = 1, 2, 3$, and 4 hours.

3.2 Constant Synthesis and Linear Degradation

Now we consider solutions to Equation (2) with initial conditions from Equation (3) and a constant synthesis and linear degradation model

$$I(a;\theta) = \lambda - \delta a. \tag{17}$$

Flux functions of this form have been previously used in modeling cellular populations (Flores, 2013b). In this case the DLSPM, Equation (2), no longer admits analytic solutions.

3.2.1 Recursive Integral Formulation

Applying Theorem 1, we first solve the characteristic equation

$$\frac{da}{dt} = \lambda - \delta a, \tag{18}$$

with the parametric initial condition $a(0,s) = s$. Using an integrating factor, Equation (18) has solutions

$$a(t,s) = \frac{\lambda}{\delta} + \exp(-\delta t)\left(s - \frac{\lambda}{\delta}\right) \quad \text{and} \quad s(t,a) = \frac{\lambda}{\delta} + \exp(\delta t)\left(a - \frac{\lambda}{\delta}\right).$$

Then we solve

$$\mu_i(t,s) = \exp\left(\int_0^t \alpha_i(\tau) + \beta_i(\tau) + \frac{dI(a;\theta)}{da}\Big|_{a=a(\tau,s)} d\tau\right).$$

This is simply $\mu_i(t,s) = \exp\left(\int_0^t \alpha_i(\tau) + \beta_i(\tau) - \delta d\tau\right)$. The dynamics of the initial generation are then given by the equation

$$Y_0(t,a) = \mu_0(t,s(t,a))^{-1}\Upsilon\left(\frac{\lambda}{\delta} + \exp(\delta t)\left(a - \frac{\lambda}{\delta}\right)\right). \tag{19}$$

Continuing with Theorem 1, $Y_i(t,a)$ is then given by the recursive equation

$$Y_i(t,a) = \frac{2\gamma\alpha_{i-1}(t)}{\mu_i(t,s(t,a))}\int_0^t \mu_i(\tau,s(t,a))Y_{i-1}(\tau,\gamma a(\tau,s(t,a)))d\tau, \tag{20}$$

Method	Runtime (s)			
	$T = 1$	$T = 2$	$T = 3$	$T = 4$
LxW_1	0.04184	0.07266	0.1037	0.1451
LxW_2	2.926	5.497	8.533	11.27
RNI	106.1	109.3	252.6	254.6

Table 3: **Numerical Runtimes Constant Growth and Linear Decay.** Comparison of runtimes for numerical solutions (LxW and RNI) for the DLSPM (Equations (2)–(3)) with constant growth and linear decay (Equation (17)) at four different model evaluation times $T = 1, 2, 3$, and 4 hours.

for $i > 0$. Thus, the first generation dynamics are given by the equation

$$Y_1(t,a) = \frac{2\gamma\alpha_1(t)}{\exp\left(\int_0^t \alpha_1(\tau) + \beta_1(\tau) - \delta d\tau\right)} \int_0^t \exp\left(\int_0^t \alpha_1(\tau) + \beta_1(\tau) - \delta d\tau\right) Y_0(\tau, \gamma a(\tau, s(t,a)))d\tau. \tag{21}$$

Here, substitution of the term $\gamma a(\tau, s(t,a))$ in $Y_0(t,a)$ for a leads to an integral form where the existence of an analytic solution to the integral in τ depends on the form of the initial distribution Υ. Therefore, continuing inductively to determine solutions for $Y_i(t,a)$ leads to high dimensional integral equations whose dimensionality (number of nested integrals) scales with the generation (i). The formulation in Equation (20) allows for the estimate of $Y_i(t,a)$ for a particular value of intracellular constituents (a) at any time (t), without explicit knowledge of $Y_{i-1}(t,a)$.

3.2.2 Numerical Solutions

As in the linear flux case, we specify parameter values used to numerically solve our model. It is assumed that there is no cell death ($\beta_i(t) = 0$) and a time-independent rate of cell division ($\alpha_i(t) = \log(2)/1.5$). The flux term parameter values used are $\lambda = 1.5$ and $\delta = \frac{20}{1.5}$. We solved our system up to the seventh generation, $M = 7$. We set initial intracellular density $\Upsilon(a)$ to follow a normal distribution with mean 10 and a variance 1, and we begin with 10 cells in the initial population.

We compare solutions with RNI using Theorem 1 to application of LxW on the original DLSPM, Equation (2). The CFL condition for stability of the LxW method requires that our timestep be $\Delta t < \frac{\Delta a}{(M+1)\cdot \max_a\{\lambda - \delta a\}} = \frac{\Delta a}{(M+1)\lambda}$. The spatial discretizations for Lax-Wendroff for comparison with RNI are $\Delta a = 0.1$ (LxW_1) and $\Delta a = 0.01$ (LxW_2). The number of quadrature points used in our implementation of RNI and our systematic way of determining them are presented in the Appendix. Recursive numerical integration is applied on the same intracellular constituent values as LxW_1.

We show our numerical solutions in two contexts, first as each generation separately plotted (Figure 3) and then as the sum over all generations (Figure 4), which is consistent with what would be obtained with an experimental assay. While we can no longer compare with an exact solution, we see that RNI achieves results comparable to a higher order LxW method at the cost of longer runtimes than both LxW implementations. These longer runtimes for RNI are due to an increasing trend in necessary quadrature points as we estimate later generations, see the Appendix. We hypothesize that this increase in quadrature points is necessary due to the constant synthesis term in Equation (17), which adds to the recursive computational complexity of the problem.

3.3 Logistic Growth

Finally, we consider solutions to Equation (2) with initial conditions from Equation (3) with intracellular dynamics driven by logistic growth

$$I(a;\lambda,K) = \lambda a\left(1 - \frac{a}{K}\right). \tag{22}$$

The logistic equation is a standard model in mathematical biology and considers growth within a resource limited environment (Edelstein-Keshet, 2005; Segel and Edelstein-Keshet, 2013). It is characterized by two parameters λ, the maximum growth rate, and K, the maximum possible concentration. As in our previous example, Equation (2) does not admit analytic solutions. Therefore, we begin by solving for the recursive formulation and then compare numerical solutions with RNI to LxW.

3.3.1 Recursive Integral Formulation

We consider solutions to Equation (2) with initial conditions given in Equation (3) under logistic growth (Equation (22)). As before, following Theorem 1, we first solve the characteristic equation

$$\frac{da}{dt} = \lambda a\left(1 - \frac{a}{K}\right),$$

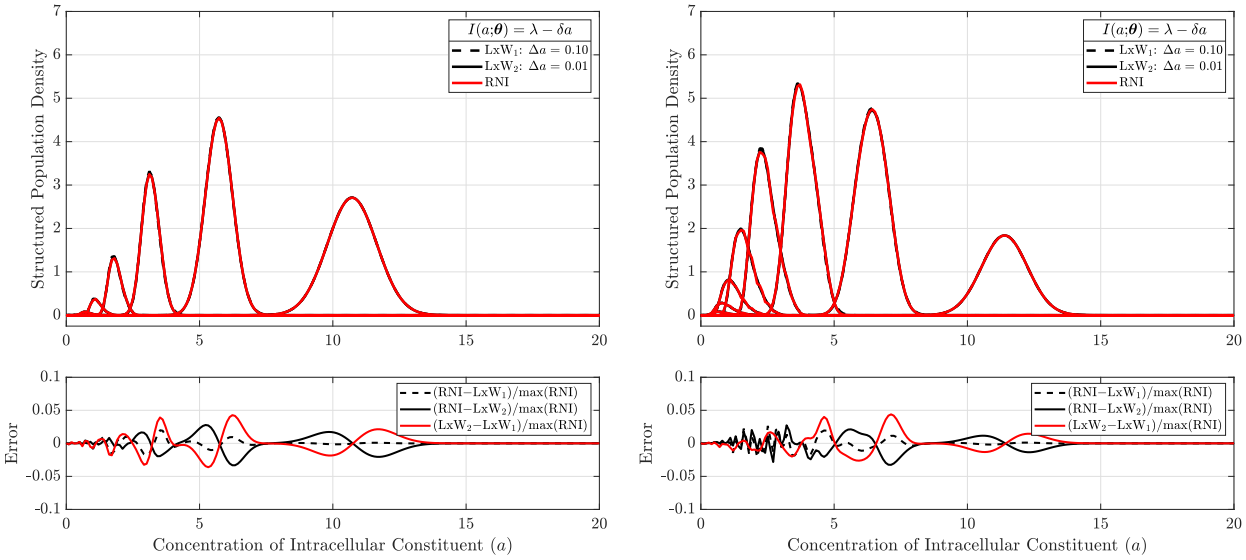

(a) $T = 1$ hour of experimental time.

(b) $T = 2$ hours of experimental time.

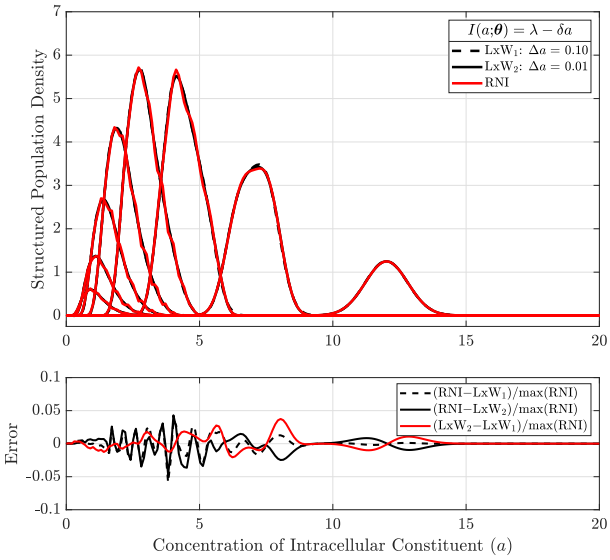

(c) $T = 3$ hours of experimental time.

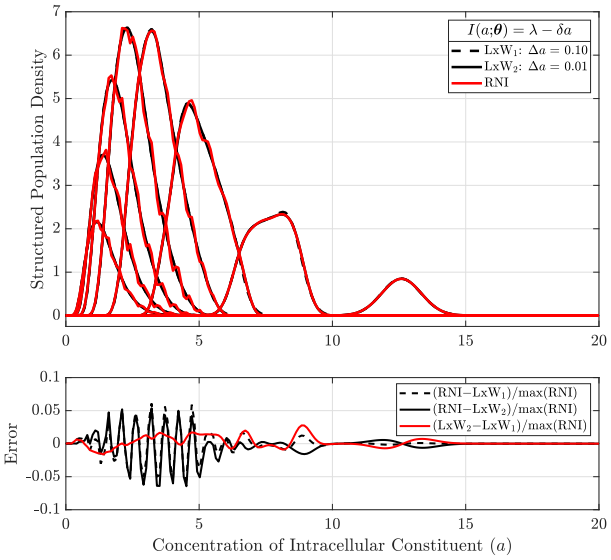

(d) $T = 4$ hour of experimental time.

Figure 3: **Numerical Solutions Constant Growth and Linear Decay: Separate Generations.** We compare numerical solutions (RNI, LxW) of the DLSPM, (Equations (2)–(3)) with Flux Term (Equation (17)). (Top) We separately plot each generation at different points in time $T = 1, 2, 3$, and 4 hours. For the LxW method we used a uniform mesh with $\Delta a = 0.1$ (LxW$_1$) and $a = 0.01$ (LxW$_2$), and we used $\Delta a = 0.01$ for the RNI method. (Bottom) The error between the RNI and LxW solutions. (See Section 3.2 for further details).

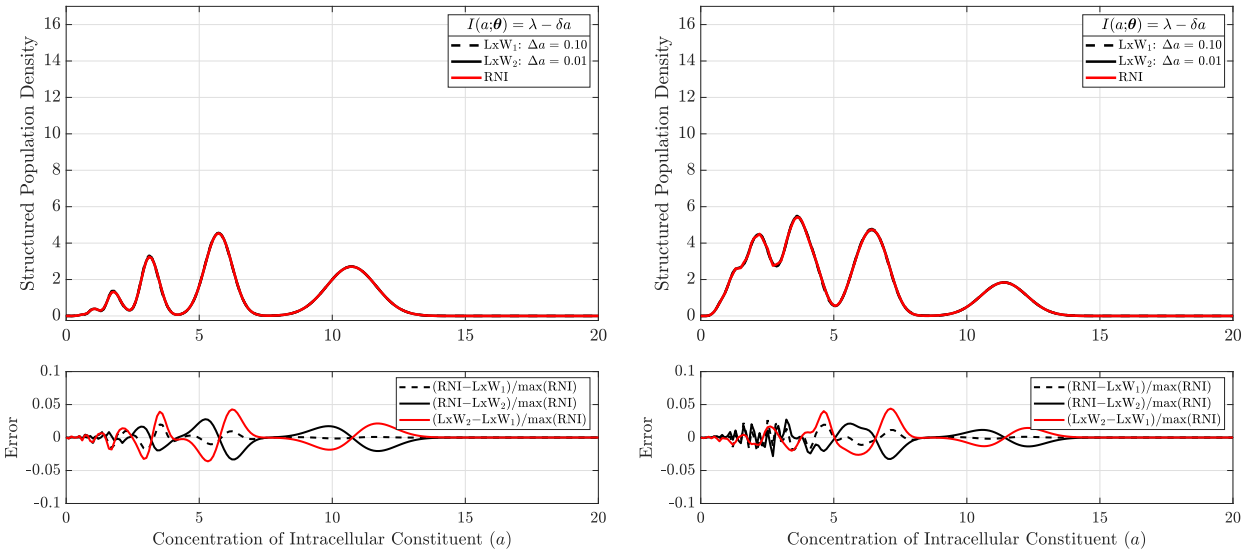

(a) $T = 1$ hour of experimental time.

(b) $T = 2$ hours of experimental time.

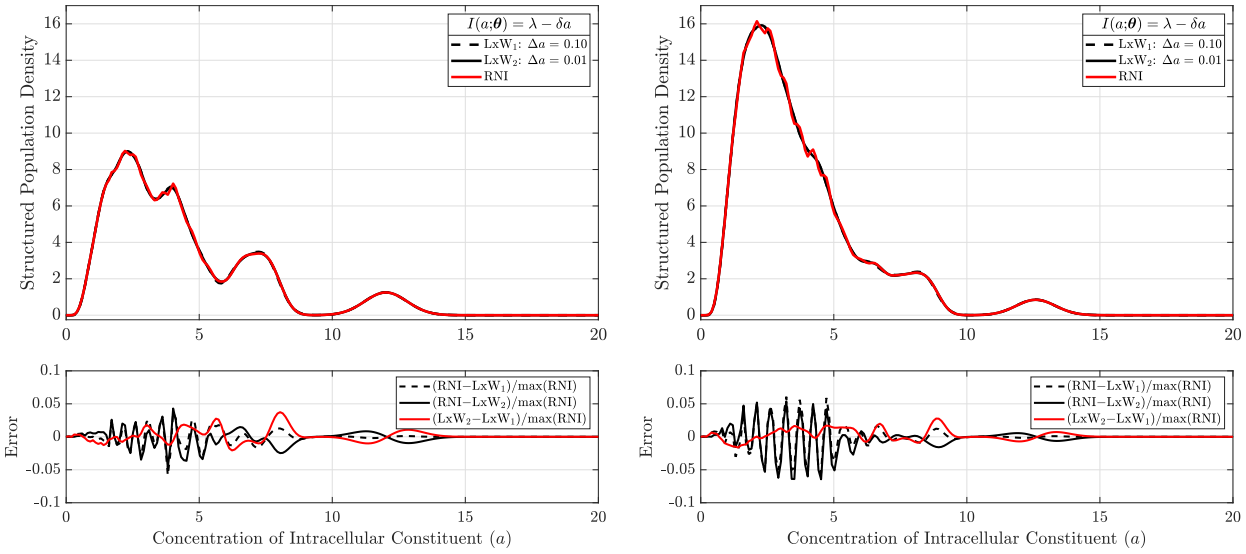

(c) $T = 3$ hours of experimental time.

(d) $T = 4$ hour of experimental time.

Figure 4: **Numerical Solutions Constant Growth and Linear Decay: Total Population.** We compare numerical solutions (RNI, LxW) of the DLSPM, (Equations (2)–(3)) with Flux Term (Equation (17)). (Top) We plot the sum of all generations at different points in time $T = 1, 2, 3$, and 4 hours. For the LxW method we used a uniform mesh with $\Delta a = 0.1$ (LxW$_1$) and $a = 0.01$ (LxW$_2$), and we used $\Delta a = 0.01$ for the RNI method. (Bottom) The error between the RNI and LxW solutions. (See Section 3.2 for further details).

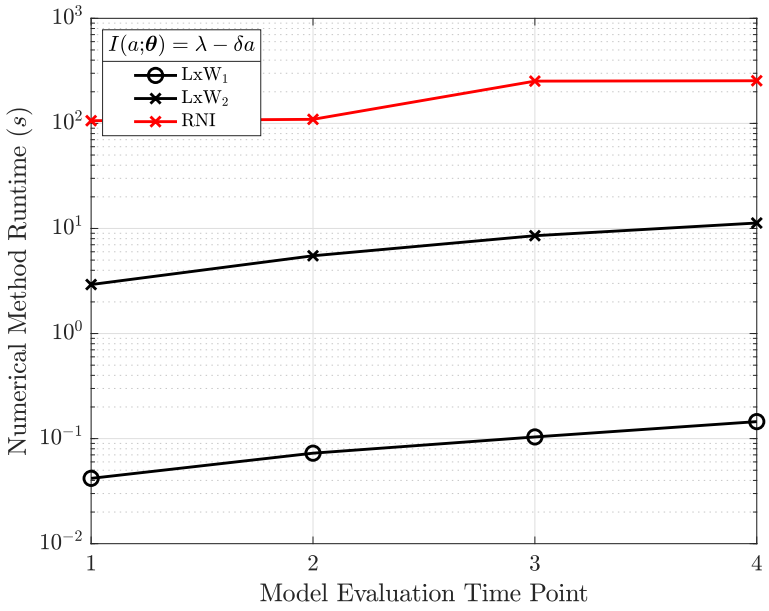

Figure 5: **Numerical Runtimes Constant Growth and Linear Decay.** Comparison of runtimes for numerical solutions (LxW and RNI) for the DLSPM (Equations (2)–(3)) with constant growth and linear decay (Equation (17)) at four different model evaluation times $T = 1, 2, 3$, and 4 hours.

with the parametric initial condition $a(0, s) = s$. This has solutions

$$a(t,s) = \frac{Ks\exp(\lambda t)}{K - s + s\exp(\lambda t)} \quad \text{and} \quad s(t,a) = \frac{Ky}{a - a\exp(\lambda t) + K\exp(\lambda t)}.$$

Secondly, we solve for $\mu_i(t, s(t,a))$ by

$$\mu_i(t,s(t,a)) = \exp\left(\int_0^t \alpha_i(\tau) + \beta_i(\tau) + \frac{dI(a;\theta)}{da}\Big|_{a=a(\tau,s)} d\tau\right),$$

so that

$$\mu_i(t,s(t,a)) = \left(\frac{K}{K + s(t,a)(\exp(\lambda t) - 1)}\right)^2 \exp\left(\lambda t + \int_0^t \alpha_i(\tau) + \beta_i(\tau) d\tau\right).$$

We have an analytic solution for the initial generation, $Y_0(t,a) = \mu_0(t,s(t,a))^{-1}\Upsilon\left(\frac{Ky}{a - a\exp(\lambda t) + K\exp(\lambda t)}\right)$. Then, continuing with Theorem 1, $Y_i(t,a)$ is given by the recursive equation

$$Y_i(t,a) = \frac{2\gamma\alpha_{i-1}(t)}{\mu_i(t,s(t,a))} \int_0^t \mu_i(\tau,s(t,a)) Y_{i-1}(\tau, \gamma a(\tau,s(t,a)))d\tau, \tag{23}$$

for $i > 0$. However, we no longer obtain non-integral solutions for $Y_i(t,a)$ for any initial distribution Υ by inductively using the previous solution $Y_{i-1}(t,a)$ by substituting the term $Y_{i-1}(t, \gamma a(t,s(t,a)))$ in the integral form of $Y_i(t,a)$. In this case, substitution of $Y_{i-1}(t, \gamma a(t,s(t,a)))$ leads to high dimensional integral solutions for $Y_i(t,a)$, whose dimension depends on the generation (i). The advantage to numerically solving the formulation in Equation (23), over numerically solving the system in Equation (2), is that for later generations, we can estimate this solution for a particular value of intracellular constituents (a) at any time (t).

3.3.2 Numerical Solutions

In our numerical solutions, we assume there is no cell death ($\beta_i(t) = 0$) and a time-independent rate of cell division ($\alpha_i(t) = \log(2)/1.5$). We fix the parameters in the logistic model: $\lambda = 1.5$ and $K = 20$. The number of initial cells was set equal to 1 and the initial population density, $\Upsilon(a)$ was set to a normal distribution with mean 1 and variance 0.1. We solved our system up to generation $M = 7$.

Method	Runtime (s)			
	$T = 1$	$T = 2$	$T = 3$	$T = 4$
LxW_1	0.2158	0.358	0.5186	0.6939
LxW_2	13.71	26.52	37.91	49.82
RNI	0.1069	0.2391	0.1237	0.6472

Table 4: **Numerical Runtimes Logistic Growth.** Comparison of runtimes for LxW and RNI for numerical solutions (LxW and RNI) for for the DLSPM (Equations (2)–(3)) with logistic growth dynamics (Equation (22)) at four different model evaluation times $T = 1, 2, 3$, and 4 hours.

As before, we compare solutions with RNI to LxW. The CFL condition for stability of the explicit LxW method requires that our timestep be $\Delta t < \frac{\Delta a}{(M+1)\cdot \max_a\{\lambda a\left(1-\frac{a}{K}\right)\}} = \frac{4\Delta a}{(M+1)\lambda K}$. The spatial discretizations for Lax-Wendroff for comparison with RNI are $\Delta a = 0.1$ (LxW_1) and $\Delta a = 0.01$ (LxW_2). The number of quadrature points used in our implementation of RNI and our systematic way of determining them are presented in the Appendix. Recursive numerical integration is applied on the same intracellular constituent values as LxW_1.

As in the previous example, we show our solutions in two ways: each generation separately (Figure 6) and the sum of all generations to be more consistent with experimental results (Figure 7). Notice that our implementation of Theorem 1 with RNI achieves an accuracy that is comparable to LxW at a higher refinement ($\Delta a = 0.01$) with a much faster runtime than both LxW implementations (Figure 8 and Table 4). These also show that while LxW with $\Delta a = 0.1$ and RNI take a fraction of a second of computational time, LxW with $\Delta a = 0.01$ takes more than 100 times longer to run. We also observe that unlike in the case of constant synthesis and linear degradation (Section 3.2), application of Theorem 1 with RNI required a decreasing number of quadrature points to estimate later generations, see the Appendix.

4 Discussion & Conclusions

In this work, we presented a new theorem that gives a recursive solution to the label structured population models. This theorem applies to more general functional forms of the flux term for DLSPMs than addressed by previous work in Banks et al. (2016); Hasenauer et al. (2012) whose aims were to speed up computation of the forward solution to the PDE system with decomposition techniques. Our recursive solution structure allows us to define $Y_1(t,a)$, by using the solution $Y_0(t,a)$, then $Y_2(t,a)$ can be written by assuming that $Y_1(t,a)$ has already been defined, and so on for $i \geq 2$. For some examples, an analytic solution for each generation can be determined, as in the case of Section 3.1. In other cases our formulation allows for novel numerical solutions. We provided examples for applying this theorem with RNI to functional forms of the flux term which have been previously used to describe the production or decay of intracellular constituents, including linear growth, constant growth with linear degradation, and logistic growth. Numerical results for a DLSPM with linear flux, in which we can also compute an exact solution for a baseline comparison, showed that the RNI method was significantly more efficient than the Lax-Wendroff (LxW) finite difference method, a standard numerical technique for approximating the solution of first order hyperbolic PDE systems. We found that application of Theorem 1 with RNI was more accurate than finite differences even when a very small step size was employed with the LxW method. We observed that RNI was between 900 to 5,000 times faster than the LxW method for this base case. For flux terms with constant growth and linear degradation, we found that RNI was 36 times slower than the LxW method. However, with the more complex flux term of logistic growth, RNI was between 77 to 300 times faster than the LxW. We believe that in the case of flux terms with constant synthesis, the additive term adds to the computational complexity when applying RNI methods to evaluate the DLSPM. However, the LxW method can efficiently handle first order hyperbolic PDE systems with a constant flux term.

An advantage of using Theorem 1 and RNI is in that this leads to a meshfree method for evaluating the DLSPM for an individual point in time and an intracellular constituent amount for a particular generation. The runtimes presented in Figures 2, 5, and 8 are the result of applying RNI on the coarse spatial grid for LxW, so evaluation of the DLSPM with Theorem 1 using RNI at one point takes less time than was reported. We also explored a forward method (iterative approach) of using Theorem 1, by saving the solution to the previous generation (i) to approximate the next generation ($i+1$) in hopes that this would lead to a speedup in runtime; however, we found that this is not the case because in saving the solution to the previous generation we incur two costs. First, we incur an overhead cost from storing the previous solution by discretizing in time and space. Second, we incur additional overhead in having to use an interpolation method on previous generation in order to produce the next generation. The need for an interpolation method can be seen in the form of Equation (4) in Theorem 1 because of the $\gamma a(\tau, s(t,a))$ in the integrand

$$Y_i(t,a) = \frac{2\gamma\alpha_{i-1}(t)}{\mu_i(t,s(t,a))}\int_0^t \mu_i(\tau,s(t,a))\,Y_{i-1}(\tau,\gamma a(\tau,s(t,a)))d\tau.$$

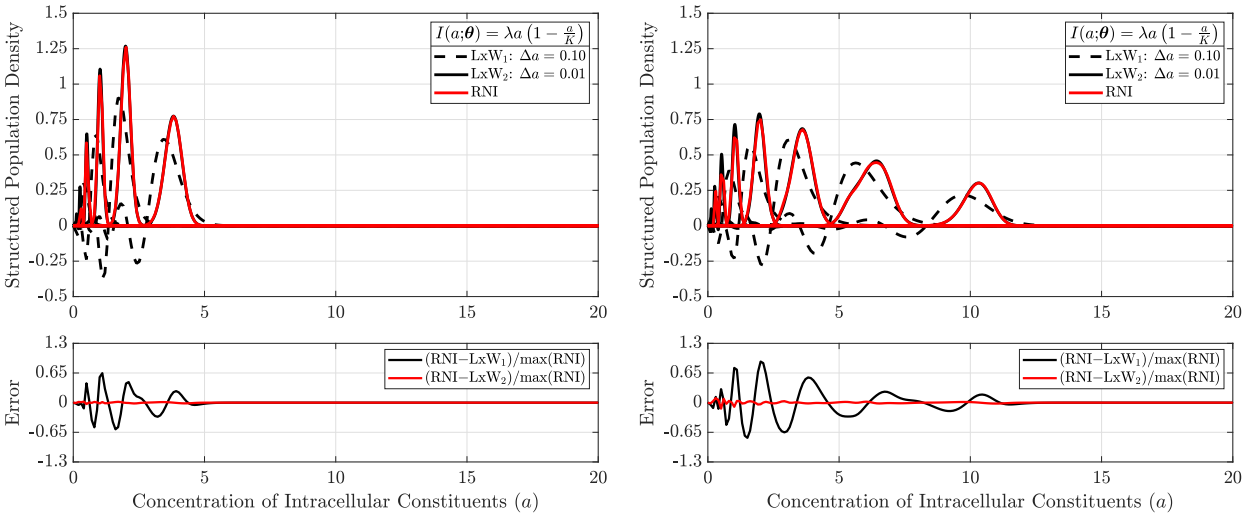

(a) T = 1 hour of experimental time.

(b) T = 2 hour of experimental time.

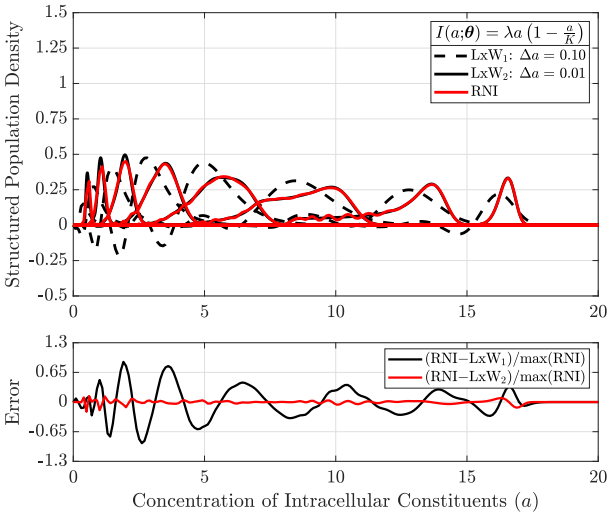

(c) T = 3 hours of experimental time.

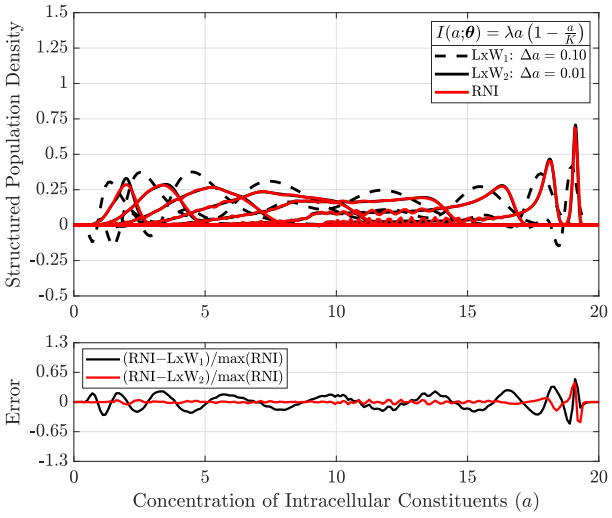

(d) T = 4 hours of experimental time.

Figure 6: **Numerical Solutions Logistic Growth: Separate Generations.** We compare numerical solutions from (RNI and LxW) of the DLSPM (Equations (2)–(3)) with Flux Term (Equation (22)). (Top) We separately plot each generation at different points in time T = 1, 2, 3, and 4 hours. For the LxW method we used a uniform mesh with Δa = 0.1 (LxW$_1$) and a = 0.01 (LxW$_2$), and we used Δa = 0.01 for the RNI method. (Bottom) The error between the RNI and LxW solutions. (See Section 3.3 for further details).

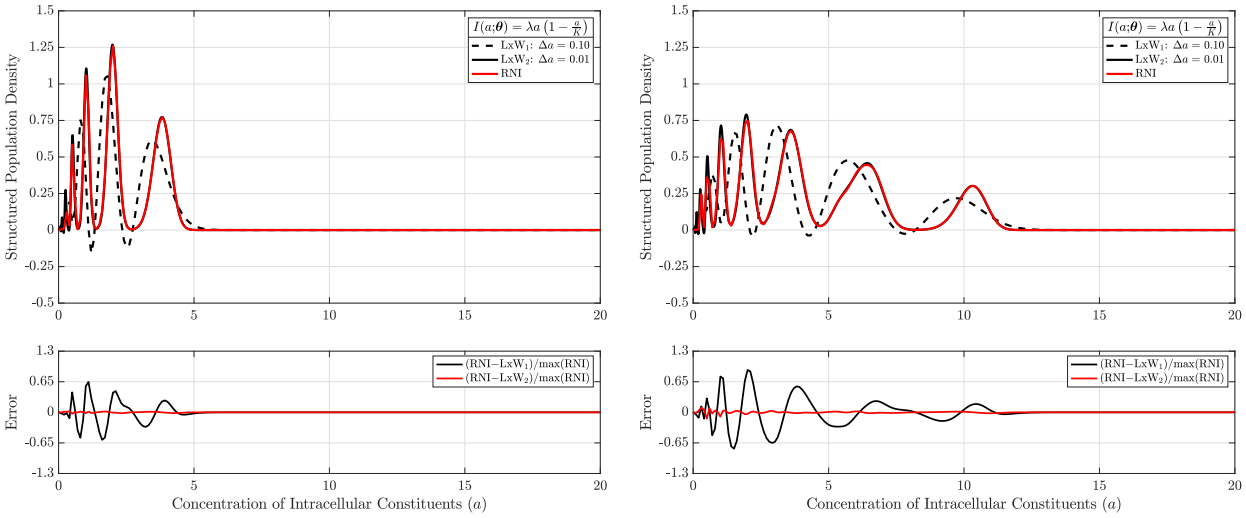

(a) $T = 1$ hour of experimental time.

(b) $T = 2$ hour of experimental time.

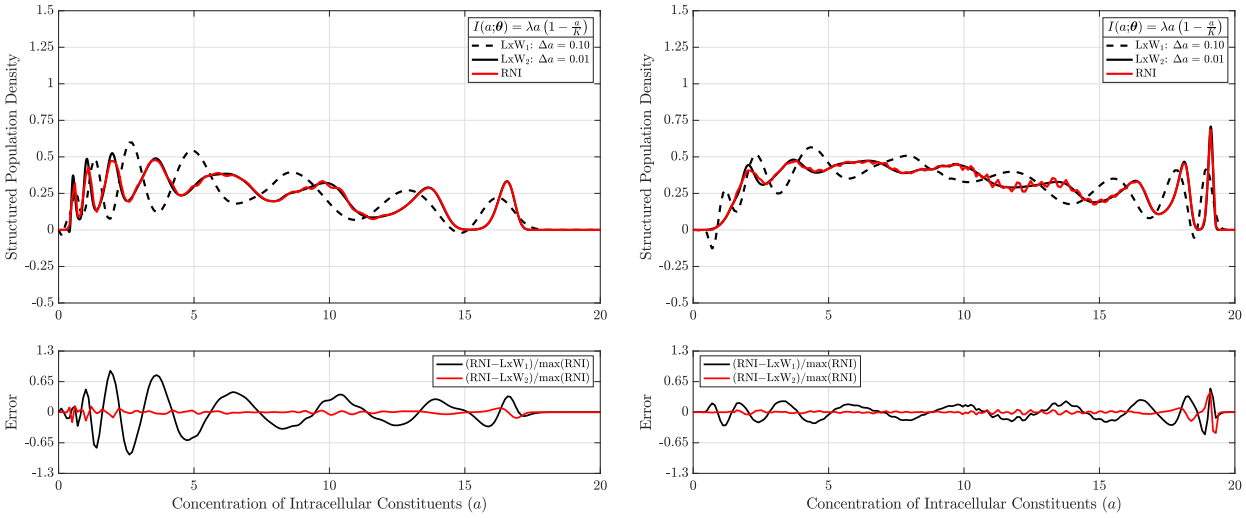

(c) $T = 3$ hours of experimental time.

(d) $T = 4$ hours of experimental time.

Figure 7: **Numerical Solutions Logistic Growth: Total Population.** We compare numerical solutions from (RNI and LxW) of the DLSPM (Equations (2)–(3)) with Flux Term (Equation (22)). (Top) We plot the sum of generation at different points in time $T = 1, 2, 3$, and 4 hours. different points in time. For the LxW method we used a uniform mesh with $\Delta a = 0.1$ (LxW$_1$) and $a = 0.01$ (LxW$_2$), and we used $\Delta a = 0.01$ for the RNI method. (Bottom) The error between the RNI and LxW solutions. (See Section 3.3 for further details).

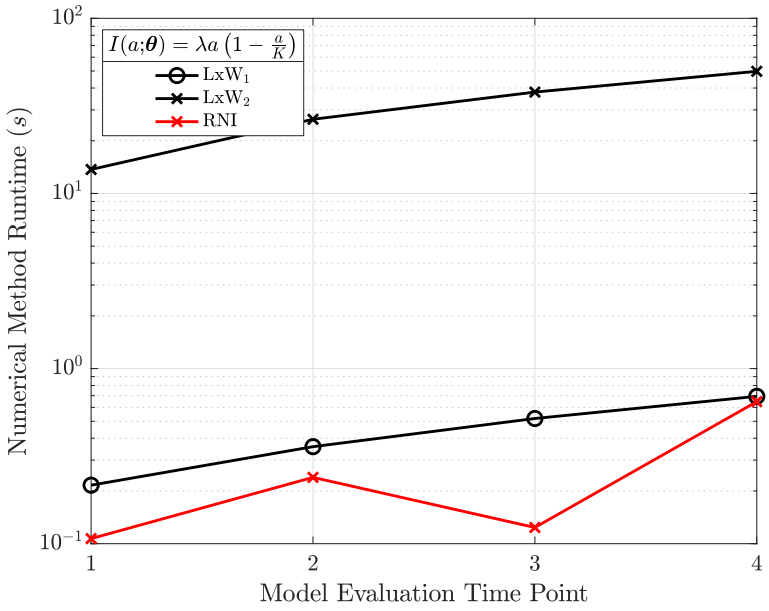

Figure 8: **Numerical Runtimes Logistic Growth.** Comparison of runtimes for LxW and RNI for numerical solutions (LxW and RNI) for for the DLSPM (Equations (2)–(3)) with logistic growth dynamics (Equation (22)) at four different model evaluation times $T = 1, 2, 3$, and 4 hours.

The RNI method on the other hand takes advantage of the recursive formulation in Theorem 1.

There are ways in which application of the RNI method can be sped up that were not considered in this work. We used Gaussian quadrature to approximate the integrals observed in the recursion formulation in Theorem 1, but there are other methods and problem specific quadrature rules that lead to greater stability and faster integration times (Weideman and Laurie, 2000). In our work, we found that generating the quadrature points during each recursive integration using the scripts from von Winckel (2004) was another limiting factor. While we do not address these problems in our work, we believe that these are problem specific details that open up other research directions.

Our results are significant because the increased efficiency will drastically speed up the ability to perform inverse problems, e.g., for parameter estimation, in which thousands of forward solutions of the entire PDE system are typically required. Thereby, Theorem 1 combined with the RNI method will enable model comparisons (Banks and Tran, 2009; Banks et al., 2018), i.e., the testing of many different model structures including more detailed molecular processes, which may have previously been unexplored due to computational burden. Moreover, RNI will enable researchers to perform uncertainty quantification for DLSPMs, since methods such as Markov Chain Monte Carlo Bayesian estimation or frequentist bootstrapping techniques can require several orders of magnitude more forward solves than parameter estimation with gradient based optimization (Kenz et al., 2013; Smith, 2014).

Code and Data

Open-source code for both RNI and LxW methods are available at `https://github.com/biomathlab/DLSPM_solver`.

Acknowledgments

This research was funded in part by the Joint Initiative to Support Research at the Interface of the Biological and Mathematical Sciences between the National Science Foundation Division of Mathematical Sciences (NSF-DMS) and National Institutes of Health National Institute of General Medical Sciences (NIH-NIGMS) (Grant No. R01-GM126548) and used the Multi-Environment Computer for Exploration and Discovery (MERCED) cluster at UC Merced, funded by National Science Foundation (Grant No. ACI-1429783); in part by the National Science Foundation (Grant Nos. DMS-1514929 and IOS-1838314) and in part by the National Institute of Aging (Grant No. R21AG059099).

References

Ammon, A., A. Genz, T. Hartung, K. Jansen, H. Leövey, and J. Volmer (2016). Applying recursive numerical integration techniques for solving high dimensional integrals. *PoS LATTICE2016*, 335. 155

Banks, H., K. B. Flores, C. R. Langlois, T. R. Serio, and S. S. Sindi (2018). Estimating the rate of prion aggregate amplification in yeast with a generation and structured population model. *Inverse Problems in Science and Engineering 26*(2), 257–279. 154, 167

Banks, H., K. L. Sutton, W. C. Thompson, G. Bocharov, D. Roose, T. Schenkel, and A. Meyerhans (2011a). Estimation of cell proliferation dynamics using cfse data. *Bulletin of mathematical biology 73*(1), 116–150. 153

Banks, H. T., K. B. Flores, and S. Sindi (2016). On analytical and numerical approaches to division and label structured population models. *Applied Mathematics Letters 60*, 81–88. 154, 164

Banks, H. T., K. L. Sutton, W. C. Thompson, G. Bocharov, M. Doumic, T. Schenkel, J. Argilaguet, S. Giest, C. Peligero, and A. Meyerhans (2011). A new model for the estimation of cell proliferation dynamics using cfse data. *Journal of immunological methods 373*(1-2), 143–160. 153

Banks, H. T., K. L. Sutton, W. C. Thompson, G. Bocharov, D. Roose, T. Schenkel, and A. Meyerhans (2011b). Estimation of cell proliferation dynamics using cfse data. *Bulletin of mathematical biology 73*(1), 116–150. 153

Banks, H. T., W. C. Thompson, C. Peligero, S. Giest, J. Argilaguet, and A. Meyerhans (2012, October). A division-dependent compartmental model for computing cell numbers in CFSE-based lymphocyte proliferation assays. *Mathematical biosciences and engineering: MBE 9*(4), 699–736. 154

Banks, H. T. and H. T. Tran (2009, January). *Mathematical and Experimental Modeling of Physical and Biological Processes*. CRC Press. Google-Books-ID: SSRapIe8p3QC. 167

Blake, W. J., M. Kærn, C. R. Cantor, and J. J. Collins (2003). Noise in eukaryotic gene expression. *Nature 422*(6932), 633–637. 154

De Boer, R. J., V. V. Ganusov, D. Milutinović, P. D. Hodgkin, and A. S. Perelson (2006). Estimating lymphocyte division and death rates from cfse data. *Bulletin of mathematical biology 68*(5), 1011–1031. 153

De Boer, R. J. and A. S. Perelson (2005). Estimating division and death rates from cfse data. *Journal of computational and applied mathematics 184*(1), 140–164. 153

Deenick, E. K., A. V. Gett, and P. D. Hodgkin (2003). Stochastic model of t cell proliferation: a calculus revealing il-2 regulation of precursor frequencies, cell cycle time, and survival. *The Journal of Immunology 170*(10), 4963–4972. 153

Edelstein-Keshet, L. (2005). *Mathematical models in biology*. SIAM. 160

Flores, K. B. (2013a, July). A structured population modeling framework for quantifying and predicting gene expression noise in flow cytometry data. *Applied Mathematics Letters 26*(7), 794–798. 154

Flores, K. B. (2013b). A structured population modeling framework for quantifying and predicting gene expression noise in flow cytometry data. *Applied mathematics letters 26*(7), 794–798. 159

Ganusov, V. V., S. S. Pilyugin, R. J. de Boer, K. Murali-Krishna, R. Ahmed, and R. Antia (2005). Quantifying cell turnover using cfse data. *Journal of immunological methods 298*(1-2), 183–200. 153

Gett, A. V. and P. D. Hodgkin (2000, September). A cellular calculus for signal integration by T cells. *Nature Immunology 1*(3), 239–244. 153

Glauche, I., K. Moore, L. Thielecke, K. Horn, M. Loeffler, and I. Roeder (2009). Stem cell proliferation and quiescence-two sides of the same coin. *PLoS Comput Biol 5*(7), e1000447. 153

Hasenauer, J., D. Schittler, and F. Allgöwer (2012). Analysis and simulation of division-and label-structured population models. *Bulletin of mathematical biology 74*(11), 2692–2732. 154, 156, 157, 159, 164

Kenz, Z. R., H. T. Banks, and R. C. Smith (2013, January). Comparison of Frequentist and Bayesian Confidence Analysis Methods on a Viscoelastic Stenosis Model. *SIAM/ASA Journal on Uncertainty Quantification 1*(1), 348–369. Publisher: Society for Industrial and Applied Mathematics. 167

Luzyanina, T., D. Roose, and G. Bocharov (2009a). Distributed parameter identification for a label-structured cell population dynamics model using cfse histogram time-series data. *Journal of mathematical biology 59*(5), 581–603. 153

Luzyanina, T., D. Roose, and G. Bocharov (2009b). Distributed parameter identification for a label-structured cell population dynamics model using cfse histogram time-series data. *Journal of mathematical biology 59*(5), 581. 153

Luzyanina, T., D. Roose, T. Schenkel, M. Sester, S. Ehl, A. Meyerhans, and G. Bocharov (2007). Numerical modelling of label-structured cell population growth using cfse distribution data. *Theoretical Biology and Medical Modelling 4*(1), 26. 153, 154

Lyons, A. B., J. Hasbold, and P. D. Hodgkin (2001). Flow cytometric analysis of cell division history using dilution of carboxyfluorescein diacetate succinimidyl ester, a stably integrated fluorescent probe. In *Essential Cytometry Methods*, pp. 375–398. Wiley New York. 153

Lyons, A. B. and C. R. Parish (1994, May). Determination of lymphocyte division by flow cytometry. *Journal of Immunological Methods 171*(1), 131–137. 153

Marx, V. (2019). A dream of single-cell proteomics. *Nature methods 16*(9), 809–812. 153

Parish, C. R. (1999). Fluorescent dyes for lymphocyte migration and proliferation studies. *Immunology and cell biology 77*(6), 499–508. 153

Pinchover, Y. and J. Rubinstein (2005). *An introduction to partial differential equations*. Cambridge university press. 155

Quah, B. J., H. S. Warren, and C. R. Parish (2007). Monitoring lymphocyte proliferation in vitro and in vivo with the intracellular fluorescent dye carboxyfluorescein diacetate succinimidyl ester. *Nature protocols 2*(9), 2049. 153

Segel, L. A. and L. Edelstein-Keshet (2013). *A Primer in Mathematical Models in Biology*, Volume 129. Siam. 160

Shampine, L. F. (2005). Solving hyperbolic pdes in matlab. *Applied Numerical Analysis & Computational Mathematics 2*(3), 346–358. 155

Smith, J. and L. Martin (1973). Do cells cycle? *Proceedings of the National Academy of Sciences 70*(4), 1263–1267. 153

Smith, R. C. (2014). *Uncertainty quantification: theory, implementation, and applications*. Philadelphia: SIAM. OCLC: 875327904. 167

von Winckel, G. (2004). Legendre-gauss quadrature weights and nodes. *Matlab function lgwt. URL: http://www. mathworks. com/matlabcentral/fileexchange/4540 Wessel P, Smith WHF (1998), New, improved version of the Generic Mapping Tools released, EOS Trans. AGU 79*, 579. 156, 167

Wallace, P. K., J. D. Tario Jr, J. L. Fisher, S. S. Wallace, M. S. Ernstoff, and K. A. Muirhead (2008). Tracking antigen-driven responses by flow cytometry: monitoring proliferation by dye dilution. *Cytometry Part A 73*(11), 1019–1034. 153

Weideman, J. and D. Laurie (2000). Quadrature rules based on partial fraction expansions. *Numerical Algorithms 24*(1-2), 159. 167

Witkowski, J. M. (2008). Advanced application of cfse for cellular tracking. *Current Protocols in Cytometry 44*(1), 9–25. 153

Appendix: Determining Number of Quadrature Points

In the analysis presented in the main text, in the implementation of Recursive Numerical Integration, the number of quadrature points used (RNI_q) were chosen such that the addition of a quadrature point (RNI_{q+1}) no longer led to an improvement in the solution with a tolerance of $tol = 10^{-1}$, using an adjusted ∞-norm (see Figure 9). That is the number of quadrature points (q) used in the text satisfy $||\mathrm{RNI}_q - \mathrm{RNI}_{q+1}||_\infty / \max(\mathrm{RNI}_{q,q+1}) < tol$, for each generation and point in time presented. Here the norm adjustment term $\max(\mathrm{RNI}_{q,q+1})$ allows dynamically adapting the norm to each generation.

Tables 5–7 present the number of quadrature points used for each flux term at each point in time. Note that we have an analytic solution for the initial generation (Y_0) and so we do not use RNI to approximate this solution.

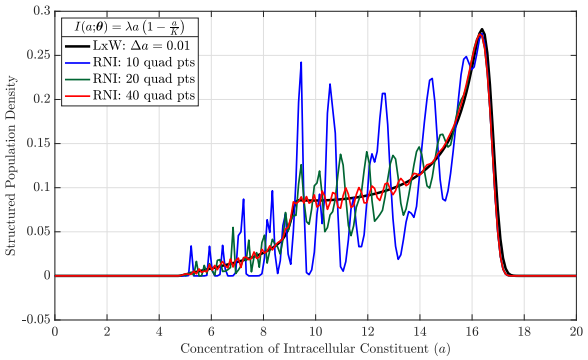

(a) Numerical solutions using Lax-Wendroff and three examples of RNI using a different number of quadrature points

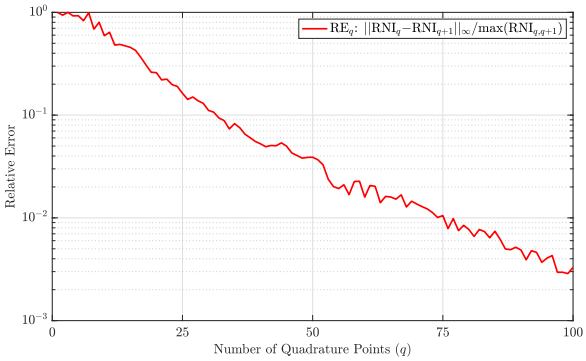

(b) The convergence of RNI as we increase the number of quadrature points

Figure 9: **Number of Quadrature Points and Convergence.** Using a logistic flux term, the concentration of intracellular constituents is determined for the second generation at four hours into the experiment. The parameter values used here are the same as in the text.

Time	**Generation**						
	Y_1	Y_2	Y_3	Y_4	Y_5	Y_6	Y_7
$T = 1$	3	3	3	3	3	4	4
$T = 2$	3	3	3	3	3	4	4
$T = 3$	3	3	3	3	3	4	4
$T = 4$	3	3	3	3	3	4	4

Table 5: **Linear Growth Flux Term.** Number of quadrature points by generation for each model evaluation time.

Time	**Generation**						
	Y_1	Y_2	Y_3	Y_4	Y_5	Y_6	Y_7
$T = 1$	3	4	6	8	10	12	14
$T = 2$	3	6	9	11	13	14	14
$T = 3$	4	7	11	13	14	14	16
$T = 4$	6	9	13	13	14	14	16

Table 6: **Constant Synthesis Linear Degradation Flux Term.** Number of quadrature points by generation for each model evaluation time.

Time	**Generation**						
	Y_1	Y_2	Y_3	Y_4	Y_5	Y_6	Y_7
$T = 1$	3	3	3	3	4	3	4
$T = 2$	5	4	4	4	4	3	5
$T = 3$	18	13	7	5	5	5	4
$T = 4$	54	33	22	13	7	7	5

Table 7: **Logistic Flux Term.** Number of quadrature points by generation for each model evaluation time.